AGU ADVANCING EARTH AND SPACE SCIENCE

Geophysical Research Letters®

RESEARCH LETTER
10.1029/2022GL098302

Mechanisms of Landslide Destabilization Induced by Glacier-Retreat on Tungnakvíslarjökull Area, Iceland

Pascal Lacroix[1,2], Joaquin M. C. Belart[3,4], Etienne Berthier[5], Þorsteinn Sæmundsson[3], and Kristín Jónsdóttir[6]

[1]ISTERRE, University Grenoble Alpes, University Savoie Mont Blanc, CNRS, IRD, UGE, Grenoble, France, [2]The Njord Centre, Department of Geosciences, University of Oslo, Oslo, Norway, [3]National Land Survey of Iceland, Akranes, Iceland, [4]Institute of Earth Sciences, University of Iceland, Reykjavík, Iceland, [5]LEGOS, CNRS, University of Toulouse, Toulouse, France, [6]Icelandic Meteorological Office, Reykjavík, Iceland

Key Points:

- We monitor the dynamics of a very large slow-moving landslide over 75 years, developing on the flank of a glaciated valley
- The landslide kinematics is strongly controlled by the glacier retreat, and produce seismicity correlated with the landslide velocity
- The acceleration is linked with progressive segmentation of the landslide mass

Supporting Information:

Supporting Information may be found in the online version of this article.

Correspondence to:

P. Lacroix,
pascal.lacroix@univ-grenoble-alpes.fr

Citation:

Lacroix, P., Belart, J. M. C., Berthier, E., Sæmundsson, Þ., & Jónsdóttir, K. (2022). Mechanisms of landslide destabilization induced by glacier-retreat on Tungnakvíslarjökull area, Iceland. *Geophysical Research Letters*, *49*, e2022GL098302. https://doi.org/10.1029/2022GL098302

Received 31 MAR 2022
Accepted 6 JUL 2022

Author Contributions:

Conceptualization: Pascal Lacroix, Joaquin M. C. Belart
Data curation: Pascal Lacroix, Joaquin M. C. Belart, Etienne Berthier
Formal analysis: Pascal Lacroix, Joaquin M. C. Belart, Kristín Jónsdóttir
Investigation: Pascal Lacroix, Joaquin M. C. Belart, Etienne Berthier, Þorsteinn Sæmundsson
Methodology: Pascal Lacroix, Joaquin M. C. Belart
Project Administration: Pascal Lacroix

Abstract The massive worldwide deglaciation leads to more frequent slope instabilities in mountainous terrains. The physical processes leading to such destabilizations are poorly constrained due to little monitoring of dynamic parameters at the local scale. Here we study a very large slow-moving landslide (~0.8 km^2), on the flank of Tungnakvíslarjökull glacier in Iceland. Based on a combination of remote sensing images, we monitor the landslide and glacier kinematics over 75 years, with a focus over the period 1999–2019 when rapid glacier wastage has been observed. The landslide accelerates from 2 to 45 m/yr in the 6 years following a sudden increase in glacier mass loss. This acceleration coincides with intense quake activity ($M_\ell < 2.8$), recorded by a regional seismic network. We show that this seismicity is caused by the landslide sliding on a rough surface. The evolution of the quake magnitudes suggests a progressive segmentation of the landslide mass during its acceleration.

Plain Language Summary Glacier-retreat may lead to a destabilization of adjacent slopes that can evolve into large landslides. The time-scales, as well as the controlling factors of the landslide response to this glacier retreat are poorly known, due to few observations of landslide dynamics in the vicinity of glaciers over the long term. To fill this gap, we document the dynamics of a large landslide in Iceland, developing on the flank of Tungnakvíslarjökull glacier, that underwent strong retreat after 1994. Based on aerial images since 1945 and satellite images since 1987, we calculate the motion of the landslide through time. We show that the landslide accelerated from 2 to 45 m/yr in the 6 years following the onset of glacier retreat. This acceleration coincides with earthquakes of small magnitudes ($M_\ell < 2.8$), produced by the landslide motion. Their analysis suggests that the landslide mass is progressively fragmented during the acceleration. This study opens interesting perspectives for landslide studies by combining seismic records from regional networks and 3D motions from satellites.

1. Introduction

Over the last decades, global warming led to massive glacier retreat over all the continents (Hugonnet et al., 2021; Zemp et al., 2019). This glacier retreat can produce geomorphologic hazards with increase occurrence of rock-falls and deep-seated landslides (Ben-Yehoshua et al., 2022; Huggel et al., 2012; McColl, 2012; McColl & Davies, 2013), that in turn can lead to potential tsunamis in fjords (Dai et al., 2020), debris flows or unstable valley dams that can evolve into lake outbursts floods (Cook et al., 2018). This chain of hazards motivates studying the physical processes leading to the slope destabilizations and the time-scales of the slope motion initiations following glacier losses.

Different studies show that the time-scales of rockslopes response to deglaciation is distributed over several tens to thousands of years, with a frequency of failure declining with time after deglaciation (Cruden & Hu, 1993; Evans & Clague, 1994; Soldati et al., 2004). These observations support the idea of debuttressing as the main control of landslide formation. Other observations show the complex combined effect of slope debuttressing with climatic forcings (Huggel et al., 2012; Zerathe et al., 2014), ice loading history (Grämiger et al., 2017), and the role of ice-thaw in fractures, that contributes to the stability of landslides (Hilger et al., 2021). Other forcings include the increase of pore water pressure in fractures at depth due to ice melting (Chiarle et al., 2021).

Software: Pascal Lacroix, Joaquin M. C. Belart, Etienne Berthier
Supervision: Pascal Lacroix
Validation: Pascal Lacroix, Etienne Berthier, Þorsteinn Sæmundsson
Visualization: Pascal Lacroix, Joaquin M. C. Belart, Etienne Berthier, Kristín Jónsdóttir
Writing – original draft: Pascal Lacroix
Writing – review & editing: Pascal Lacroix, Joaquin M. C. Belart, Etienne Berthier, Þorsteinn Sæmundsson, Kristín Jónsdóttir

Modeling also suggests various time-dependencies of the landslide kinematics to glacier debuttressing. For instance, due to the viscous nature of ice at low strain-rates, landslide motion can initiate even in the presence of a glacier and deform the latter (McColl & Davies, 2013; Storni et al., 2020). Other studies suggest that slope debuttressing leads to progressive damage and maturation of faults, associated with a time-lag of the landslide response to the glacier retreat (Ballantyne & Stone, 2004; Lacroix & Amitrano, 2013). One key aspect of this temporal dependence seems to be the time-scale of the slope damage compared to the glacier retreat velocity (Lacroix & Amitrano, 2013), the valley-shape (Spreafico et al., 2021), the landslide size (McColl & Davies, 2013) and the rheology of the ice (Storni et al., 2020). In the meanwhile, the ice-loading over repeat glacial cycles at scales thousands of years are critical to develop rock damage into the massif (Grämiger et al., 2017). Deciphering the complex combination of the physical processes and their time-scales leading to slope destabilization in periglacial environment requires more detailed observations on specific active landslides.

Recent investigations of two large deep-seated slow-moving landslides, show the direct link between glacier retreat and landslide accelerations over the Moosfluh landslide in Switzerland (Kos et al., 2016), and on the Barry Arm fjord landslide in Alaska (Dai et al., 2020). The observations of these two landslides show the stabilization role of the glacier on the slope toe, but also a delay of several years of the landslide response to the glacier retreat (Kos et al., 2016). Change of the mechanisms of deformation from toppling to sliding is also observed during this phase of acceleration on the Moosfluh landslide using in situ measurements of the landslide kinematics (Glueer et al., 2019). All these studies focus on the kinematics of the landslide and the glacier. Other physical parameters of the landslide dynamics (e.g., seismicity, elastic properties variations) would be required to decipher the mechanical processes leading to the landslide acceleration and the time-scales of the slope damage. These physical parameters can be obtained by local or distant setup of seismometers, recording both the seismicity generated by the landslide dynamics (Helmstetter & Garambois, 2010; Provost et al., 2018) and the changes of the landslide material properties from ambient noise analysis (Bontemps et al., 2020; Le Breton et al., 2021). However these setups dedicated to landslide monitoring are very seldom, and the use of regional seismic networks has often been limited by their large distance to the landslide areas, despite some promising recent results (Cook et al., 2021; Poli, 2017).

Here we document the kinematics and seismic activity of a very large deep-seated landslide in Iceland, next to Tungnakvíslarjökull outlet glacier that underwent strong retreat after 1995. These two parameters are analyzed to better study the physical processes of landslides (sliding, fracturation, glacier buttressing) forced by glacier retreat.

2. Study Site

The study site is located on the western flank of Katla central volcano, which has a 10 km wide and up to 750 m deep caldera, filled with ice (Björnsson et al., 2000). The landslide affects the slope north of Tungnakvíslarjökull, an outlet glacier of Mýrdalsjökull ice cap, S-Iceland. It spans 600 m in height reaching up to 1100 m a.s.l. The headscarp of the slide is around 2 km long (Figure 1), delimitating a total displaced area of around 0.8 km^2. The bedrock is predominantly composed of basaltic and intermediate hyaloclastite formations, interbedded with silicic extrusive (Lacasse & Garbe-Schönberg, 2001; Torfason & Jónsson, 2005). In the unstable slope north of Tungnakvíslarjökull a thick and extensive rhyolitic lava formation can be traced along the entire slope which then continues northward along the western flank of the ice cap. The age of this formation is expected to be in the range of 10 ,000–55 000 years, but it is not known whether it is subaerial or intrusive in origin. This formation is then capped with hyaloclastite (Torfason & Jónsson, 2005). The landslide was discovered recently, and a permanent GNSS was installed in 2020 to monitor its activity (https://notendur.hi.is/hgeirs/iceland_gps/icel_tkjs.html).

As the other southern outlets of Mýrdalsjökull and nearby Eyjafjallajökull ice cap (Belart et al., 2019), Tungnakvíslarjökull has a maritime regime with high mass balance sensitivity to climate, reflected by its high mass balance amplitude (Ágústsson et al., 2013), and its rapid front variations and glacier elevation changes. It therefore adjusts more rapidly than other continental glaciers located inland or in the north to a changing climate (Belart et al., 2020; Hannesdóttir et al., 2020).

As all other outlet glaciers in Iceland, Tungnakvíslarjökull has retreated substantially from its maximum extent at the end of the Little Ice Age (LIA, ca 1890). The entire Mýrdalsjökull ice cap lost an area of 216 km^2 from 1890 to 2019 (Hannesdóttir et al., 2020). In the 1960s the retreat phase was halted and the glacier thickened and

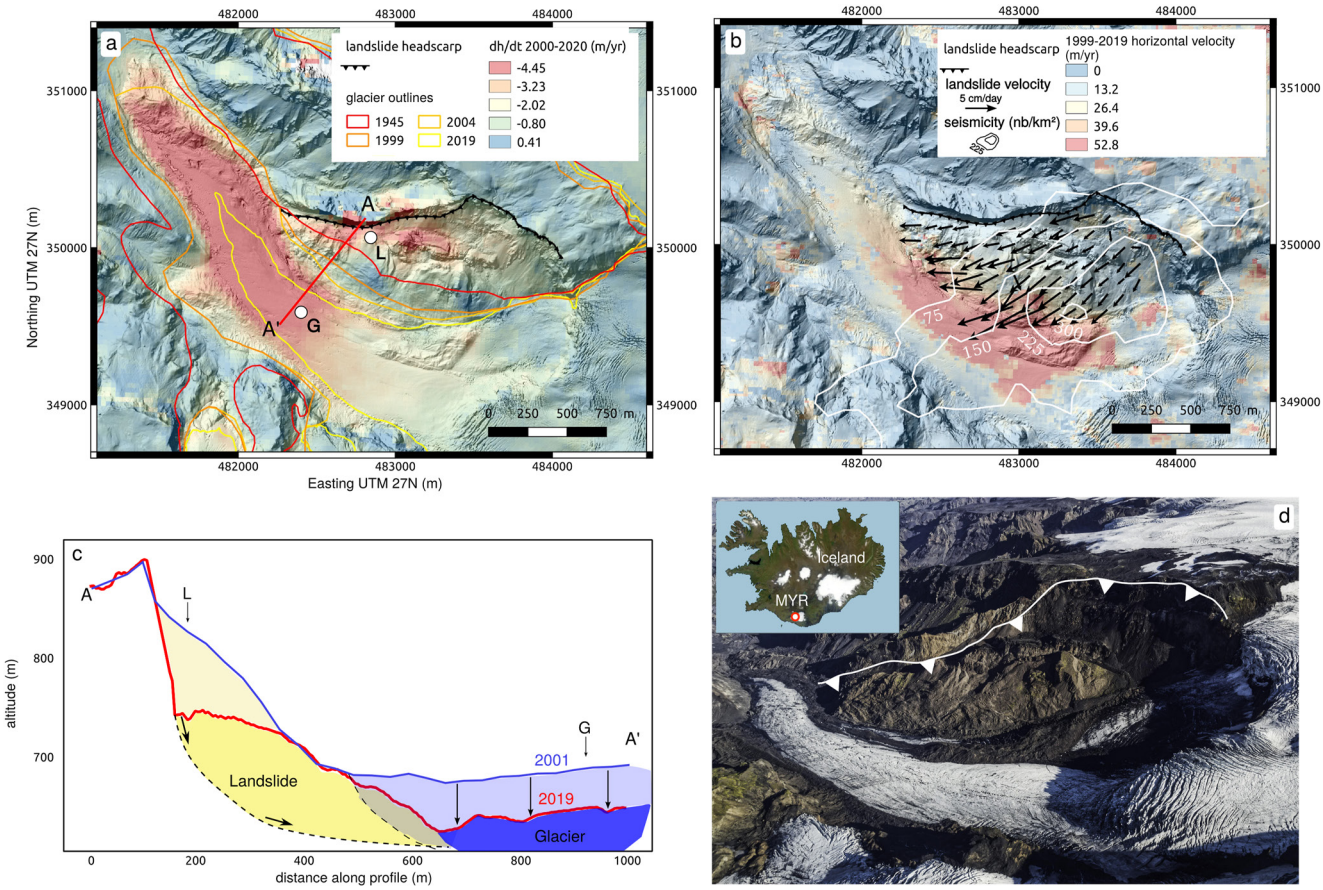

Figure 1. Vertical (a) and Horizontal (b) ground motion over Tungnakvíslarjökull and surroundings. The vertical component is a mean over the 2000–2020 period. The horizontal velocity is a mean over the 1999–2019 period. The two points L and G locate the time-series of vertical displacement shown in Figure 2. On panel b the black arrows represent the landslide velocity fields. The white lines on Panel b correspond to isolines of seismic activity (number of shallow (≤5 km) quakes per km^2 over the period 1995–2019) detected and located by the SIL network (Jónsdóttir et al., 2009). Panel c is an interpretative cross-section along the profile A-A' shown in Panel (a) Topographic profiles are extracted from the ASTER DEM time-series. Panel d represents an aerial photograph of the area taken in August 2012 (credits: Grétar Ívarsson). The landslide headscarp is highlighted with a black line in Panel a and b, a white line on Panel (d).

advanced until 1994. Then another phase of rapid retreat and thinning started and lasted up to around 2010. In the past decade (2010–2019) the glacier has shown a slightly less negative mass balance (Aðalgeirsdóttir et al., 2020; Belart et al., 2020; Hugonnet et al., 2021). Geodetic mass balance observations indicate the strongest mass loss of Mýrdalsjökull during 1999–2004, with an average mass balance of -2.4 ± 0.3 m w.e. a^{-1} (Belart et al., 2020). A series of maps of elevation changes of Mýrdalsjökull ice cap, 1960–2016, including Tungnakvíslarjökull catchment, can be found in the Supplement S8 of Belart et al. (2020).

3. Methodology

3.1. Surface Elevation Changes

Elevation changes of the glacier and landslide areas were measured using time-series of digital elevation models (DEMs) derived from aerial photographs and ASTER images (Table S1 in Supporting Information S1). Aerial photographs were processed using the MicMac software (Rupnik et al., 2017) following the guidelines presented in Belart et al. (2019). The bulk of the archives of aerial photographs in the area of study were processed in Belart et al. (2020), resulting in a series of DEMs co-registered to a lidar DEM acquired in 2010 (Johannesson et al., 2013). We also added into this time-series the aerial photographs from 1945, 1989 and 1994 (National Land Survey of Iceland) and 2004 (acquired by the private company Loftmyndir efh.). Uncertainties in individual elevation measurements from the aerial photographs range from 1 m (the oldest photographs) to 0.3 m (the newest photographs), based on similar datasets analyzed in previous studies (Belart et al., 2019, 2020).

To densify the time-series over the last 20 years, 160 satellite DEMs were generated from ASTER stereo imagery acquired between May 2000 and July 2020 with different initial coverage and data voids due to clouds or poor image correlation. Typically 30–60 ASTER elevation values are available to describe the temporal evolution of the landslide or the glacier tongue. ASTER DEMs were processed using the Ames Stereo Pipeline (ASP (Shean et al., 2016)), using the same setup as in Brun et al. (2017). Each DEM was then horizontally and vertically co-registered to the 2010 lidar DEM by minimizing the standard deviation of the elevation difference on stable terrain, that is, after excluding the glacier and landslide areas (Berthier et al., 2007). A 5th order polynomial was then fitted to the residuals along and across the satellite track (Gardelle et al., 2013) to remove elevation biases due to along and across track undulations in the ASTER DEMs (Girod et al., 2017). Uncertainties in individual ASTER elevation measurements (as quantified by the Normalized median absolute deviation) are on the order of 5–10 m.

3.2. Horizontal Ground Displacements

A time-series of horizontal displacement fields was calculated using a combination of medium-resolution images, that provide a large number of images since the 1980s. A SPOT-1 image of 10-m resolution acquired in 1987 was first orthorectified using the cosi-corr module (Leprince et al., 2007). The rigorous model of the camera was refined from a set of ground control points collected on stable areas in a recent Landsat-8 image and the lidar DEM acquired in 2010. Then 15-m resolution Landsat-7 and 8 images 1C products were used to cover the period 1999–2019 with homogeneous radiometry, geometry and resolution. One image per year was chosen based on the lack of snow and clouds at the end of the summer season (Table S1 in Supporting Information S1). Similar months of acquisitions were chosen also to limit the artifacts produced by shadows on the image correlation (Lacroix et al., 2019). Landsat-7 images after 2003 contain scan line errors, which strongly affects the correlation between two images (Rosenau et al., 2015). So these images are not used in our study after 2003, and the gap of data was filled with five ASTER images of 15-m resolution, orthorectified with their concomittent DEM (see previous section). To validate the use of ASTER images of lower radiometric resolution than Landsat-7/8 images, two ASTER images almost concomittent (less than 20 days) with Landsat-8 acquisitions were also selected (see Table S1 in Supporting Information S1).

The time-series of horizontal displacement was calculated from this time-series of Landsat/ASTER images following the approach developed in Bontemps et al. (2018): (a) correlation of all pairs of images using Mic-Mac (Rupnik et al., 2017) that is well suited to images of low radiometric contrasts or small objects (Lacroix, Dehecq, & Taipe, 2020), (b) masking the values of low correlation coefficient values (CC $\leq$ 0.65), (c) correction of coregistration bias by substracting the mean values of the NS and EW displacement fields, (d) least squares inversion of the redundant system per pixel, weighted by the time separation between pairs (Bontemps et al., 2018) that allows decreasing the motion uncertainties by about 30% of the final time-series, while keeping the initial time-resolution. This method has been validated for landslide studies of different areas using SPOT1-5 (Bontemps et al., 2018), Sentinel-2 (Lacroix, Dehecq, & Taipe, 2020), Landsat-8 (Lacroix et al., 2019) images. The uncertainties of the EW and NS displacement fields were estimated by the standard deviation of the displacement field on the stable areas (all areas outside the glaciers and the landslide) at each time-step.

3.3. Seismicity

The catalog of seismic activity analyzed in this study comes from the database produced from the South Iceland Lowland (SIL) seismic network, that has been operating with sufficient seismometers to locate events in Mýrdalsjökull since January 1995. The data contains earthquakes with a magnitude completeness of 1.7 (Jónsdóttir et al., 2007). Events are located with a horizontal and depth uncertainty of 3 and 5 km respectively. This database and its specificities are presented in details by Jónsdóttir et al. (2007); Jónsdóttir et al. (2009).Previous studies indicated a clear cluster of shallow seismic events of Magnitudes below 2.8, nearby Myrdalsjökull, with a strong seasonality pattern, and a strong increase in activity in the period 2001–2004. This unusual seismic activity questioned its origin, which was either attributed to volcanic intrusion activity (Soosalu et al., 2006) or ice-fall activity (Jónsdóttir et al., 2009). This controverse was not solved when we started the present study.

From this database, we extract the seismic events in our area of study (Figure 1b), with depth shallower than 5 km, to keep only the sources compatible with earth surface processes, and magnitudes greater than the completeness

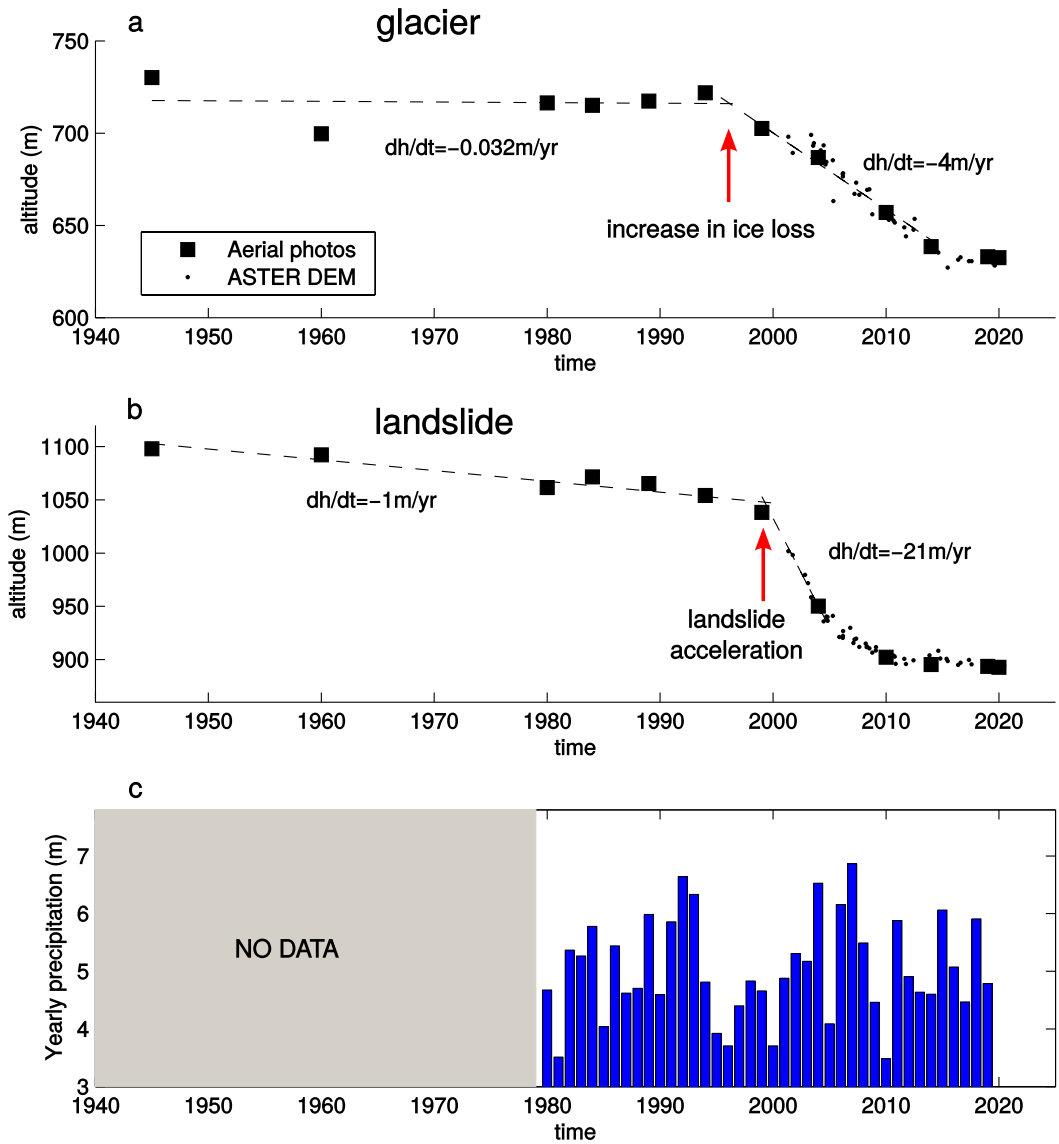

Figure 2. Time-series of elevation variations from 1945 to 2020 at two points on the glacier (a) and on the landslide (b), noted G and L on Figure 1. Velocities are estimated over time-periods where linear behaviors are observed to better estimate the timing of the acceleration onset both of the glacier ice loss and the landslide motion. Subpanel c shows the time-series of precipitation over the period 1980–2020.

magnitude of 1.7 to avoid a biased catalog. The final database analyzed here therefore contains 2089 events between January 1995 and May 2019.

4. Results

4.1. Landslide Kinematics and Seismicity

The combination of the temporally sparse estimation of the vertical displacements over 75 years and temporally resolved estimation of the horizontal displacements over the last 30 years of this period reveals successive phases of the landslide displacement (Figures 2b and 3a). The landslide headscarp subsided by roughly 1 m/yr between 1945 and 1999, before accelerating to around 21 m/yr from 2000 to 2005 (Figure 2b).

The time-series of horizontal displacement allows us to clearly distinguish different phases in this transient acceleration (Figure 3a). Between 1987 and 2001, the landslide was moving at maximum rates of 14.3 ± 4.1 m/yr on

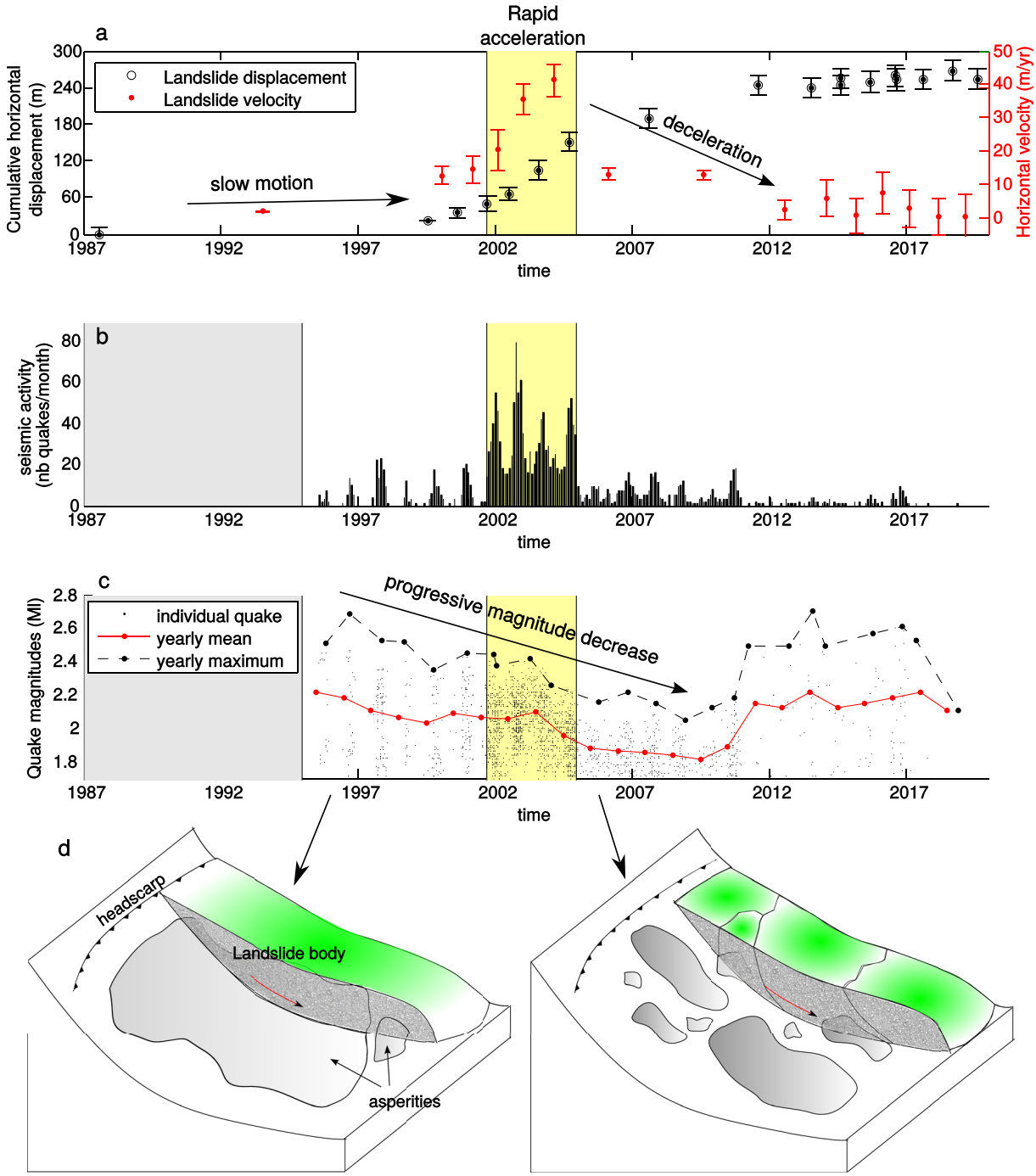

Figure 3. Time-series of geophysical parameters: (a) Horizontal cumulative displacement for a selected point on the landslide shown on Figure 1. The velocity derived from the landslide displacement time-series is shown with red colors. (b) Seismicity of the area (number of shallow quakes per month) and (c) Local magnitudes of the different quakes. The mean and maximum annual magnitudes for quakes above M$_\ell$1.7 is represented with the solid red and black dashed lines respectively. (d) Conceptual scheme of the temporal evolution of landslide fragmentation and the asperities on the landslide sliding surface.

the central part of the landslide body. Then, it suddenly accelerated over at least 3 years (September 2001–2004) to 41.2 ± 4.9 m/yr. Finally, the landslide decelerated and reached a steady state in 2011 at rates of about 3.2 m/yr, until the end of the observation period (August 2019). The 3D magnitude of the landslide velocity thus varies from 2 m/yr in the 90s to 45 m/yr in 2004, followed by a deceleration down to 3.3 m/yr from 2011 to 2019.

The landslide velocity is in the upper ranges among the slow-moving landslide velocities observed worldwide (Lacroix, Dehecq, & Taipe, 2020).

Interestingly, the seismicity of the area followed a similar pattern (Figure 3b). The seismic activity shows a strong increase between October 2001 and January 2005 compared to the 6 preceding years, followed by two successive phases of decrease (2006–2011, 2011–2019). There is a clear upper cutoff in magnitude in the seismic data set (Jónsdóttir et al., 2009). The maximum magnitudes of the quakes (Figure 3c) slowly decreased from 1995 to 2010, from 2.7 to 2.1, before increasing suddenly in 2011 to M_ℓ 2.5–2.6 until the end of the observation period (2019).

Spatially, the higher vertical velocity at the head-scarp compared to the landslide toe (Figure 1a), together with the lower horizontal velocity at the head-scarp compared to the landslide toe (Figure 1b), suggests a landslide with a rotational mechanism (Figure 1c). The sliding surface does not outcrop at the slope bottom, even at the end of the observation period (2020), where a large part of the glacier has melted. This suggests a very deep-seated landslide, with sliding surface below the glacier-bed level.

4.2. Glacier Retreat and Kinematics

Over the period 1945–1995, the elevation of the glacier tongue showed relatively small (≤1 m/yr) changes (Figure 2a), before a strong glacier wastage between 1995 and 2020. This glacier wastage is characterized by about 5 m/yr of ice elevation decrease at the landslide toe, and 50 m/yr of glacier front retreat (Figure 1a). This temporal pattern of deglaciation is shared with all the maritime glaciers in South and South East Iceland (Aðalgeirsdóttir et al., 2020; Belart et al., 2020).

The horizontal displacement field of the glacier is more complex to estimate, due to a large gap in the Landsat acquisitions between 2002 and 2014, filled only sparsely with ASTER images of lower radiometric quality than the Landsat images. This, combined to large glacier displacements in between two successive dates, make it impossible to estimate the precise time-series of displacement of the glacier. However, the displacement time-series before 2003 and after 2013 shows a linear behavior with time, allowing to calculate a mean velocity over these two periods. Lower velocities are observed after 2013 than before 2003 (See supplements, Figure S1 in Supporting Information S1), a deceleration commonly associated with glacier mass losses (Dehecq et al., 2019; Heid & Kääb, 2012). The glacier outlines also reveal a deformation of the glacier at the landslide toe (see supplements, Figure S2 in Supporting Information S1), in response to the landslide pushing.

5. Discussion

5.1. Source and Evolution of the Seismicity

The intense seismic activity which started in 2001 was first treated as volcanic unrest (Soosalu et al., 2006). Indeed, our area of study is situated on the flank of the Katla volcano, capable of explosive eruptions. In addition, the quakes are emergent, low frequency, unusually long duration events similar to those reported from volcanic environments. The absence of observed geodetic deformation (Spaans et al., 2015), the seasonality of the activity being clearly more pronounced during the wet season in the fall (Jónsdóttir et al., 2007) and the large amount of shallow (≤5 km) earthquakes likely exclude their source as volcanic. The seasonality and the location of the seismic cluster then led Jónsdóttir et al. (2009) to attribute this seismic activity to ice falls from the steep glacier. We exclude this ice-fall origin based on different criteria: (a) the magnitudes of the seismic signals would indicate very large events (Deparis et al., 2008) (because of low seismic efficiency of ice/rock falls), which is unlikely given the absence of field evidences, (b) the duration of the signals, too short (10s recorded at GOD) for a large (given the magnitude) propagating source like ice-falls (Deparis et al., 2008), (c) the absence of similar events in other glaciers in Iceland.

The presence of the landslide, discovered recently close by the seismic cluster location provides a new explanation for its origin. Despite known uncertainties, the location of the seismic cluster fits fairly well with the landslide location (Figure 1b). Its slight shift to the East of the landslide can be explained by a multitude of factors (few seismic stations, unfitted velocity models, emergent onsets of phases). Furthermore, the magnitudes of the quakes ($M_\ell \leq 2.8$), their shallow locations, the emergent waveforms (Figure S4 in Supporting Information S1) and their durations are characteristics of land-quakes (Provost et al., 2018). The seasonality of the seismic activity

also clearly indicates a seasonal process, in phase with the motion of this landslide. Indeed, the seasonal velocity measured by a GNSS installed on the landslide in June 2020 (https://notendur.hi.is/hgeirs/iceland_gps/icel_tkjs.html) peaks in October, synchronously with the seismicity (see supplements, Figure S6 in Supporting Information S1). All this combined suggests that the seismicity originates from the landslide motion. The clear cut-off magnitude observed in the seismic data likely represents a bounded deformation field in line with the interpretation that the seismicity is caused by a landslide that has a finite geometry and limited maximum slip.

The long term landslide motion (since at least 1945), at vertical rates of at least 1 m/yr, and the patterns of horizontal and vertical deformation delimited by clear scarps visible in the morphology, indicate a mechanism of sliding on a well-localized basal shear surface. On creeping landslides, the movement is not governed by the friction of the entire sliding surface, but controlled by locked sections with relatively small areas (Yamada et al., 2016). Movements on these locked areas of the heterogeneous basal-shear surface are called stick-slip events. The evidence of a well-established sliding surface, as well as the observed magnitudes and nearly identical waveforms (Figure S5 in Supporting Information S1), strongly suggest that the seismicity is created by stick-slip events over locked sections of relatively small areas during the landslide motion.

We also note that the progressive acceleration of the unstable mass is accompanied by a decrease of the maximum and mean annual quake magnitude over 15 years (1995–2010), that increase back again only after the landslide reaches a steady state in 2011 (Figure 3c). We can rule out a change of seismic attenuation along the wave path as the origin of these magnitude variations (See Supporting Information S1). Furthermore, while seismologic stress-drop estimates suffer from large uncertainties (Abercrombie, 2021), stress-drop is generally found to be independent on the earthquake magnitude (Abercrombie et al., 2016; Allmann & Shearer, 2009). Therefore the temporal evolution of the magnitude suggests a change of the characteristic rupture sizes of the earthquakes (Aki, 1966), namely a progressive decrease of the rupture size during the phase of landslide velocity changes (1996–2011), followed by a quick increase during the steady state period (2011–2019).

This observation is counter-intuitive in regards with previous studies on maturity of active faults. Indeed, accumulation of slip on the shear surface would tend to break the barriers between asperities (that can be seen as locking areas on the fault plane (Li et al., 2020; Yamada et al., 2016)), and thus leading to potential larger rupture sizes (Manighetti et al., 2007). We rather believe that this change of rupture size reflects an internal reconfiguration of the landslide during and after its acceleration period. This could suggest that the acceleration period produced a segmentation of the landslide mass (Figure 3d), with blocks progressively connected back again when the landslide reached lower velocities. This hypothesis could be confirmed by several time-series of displacement along a longitudinal profile in the landslide. Unfortunately, the low-resolution of the satellite images used here and the presence of the glacier on a large part of the landslide at the onset of the acceleration period makes it impossible to realize such differential time-series.

5.2. Landslide Kinematics Controlling Factors

The sudden and transient landslide acceleration (2001–2004) questions its triggering factor. The rapid thinning of the glacier started 5–6 years before this acceleration (Figure 2), with 40 m of thinning in this period of time. This timing suggests that glacier retreat is the major control of the landslide acceleration by debuttressing effects on valley slopes, in agreement with previous studies (Dai et al., 2020; Kos et al., 2016). Furthermore, as observed in other case-studies (Dai et al., 2020; Storni et al., 2020), the acceleration of the landslide occurs prior to the total disappearance of the glacier at the landslide toe (in 2001 the position of the glacier front is still situated 1.4 km downvalley (Figure 1a)). This suggests that the high viscosity of the ice at low strain rates allowed its deformation by the landslide over the time-scales investigated (Storni et al., 2020), which is probable given the strong flexure of the glacier at the location of the landslide toe (Figure S2 in Supporting Information S1), and/or that other factors also triggered this acceleration.

Groundwater is a major control of deep-seated landslide kinematics in general (Lacroix, Handwerger, & Bièvre, 2020). Furthermore, a damaged landslide mass, as suggested by the decrease of the rupture size with time, would ease the infiltration of surface water. However, neither the yearly cumulative rainfall in 2001, nor the cumulative seasonal rainfall in autumn 2001, present exceptional rates compared to previous years since the sudden drop in glacier elevation in 1994–1995 (Figure 2 and S7 in Supporting Information S1). Furthermore, no extreme rainfall events were observed at the onset of the landslide acceleration period in the autumn 2001, and

other extreme events are not associated with landslide accelerations (Figure S7 in Supporting Information S1). This dismisses groundwater as the final trigger of the landslide acceleration. This conclusion is also sustained by the observations at the seasonal scale. Indeed, although the peak of seasonal rainfalls almost coincides (difference by 1 month, Figure S6 in Supporting Information S1) with the peak of seismicity and velocity measured from the GNSS instruments since 2020, no peak of landslide seismicity or velocity is observed in spring/summer time during snow melt.

Other hypotheses must therefore be investigated in the future to explain the variability of the landslide kinematics after the sudden increase in glacier ice loss in 1994. For instance, we can notice that the onset of the rapid landslide motion at the end of 2001 coincides with the heaviest winter snowfall since 1994 (Figure S7 in Supporting Information S1). This questions the role of the snow-loading on the landslide kinematics. The controlling factors of the glacier buttressing on the slope should also be investigated. Indeed, the landslide accelerated before the disappearance of the glacier, and therefore the glacier buttressing still play a role in the landslide kinematics. The glacier buttressing of the slope might vary with the glacier thickness, which is inter-annually evolving, or glacier basal friction, evolving seasonally through the variations in the sub-glacial till interface and/or the subglacial water pressure (Clarke, 2005). At this stage, seasonal observations of both landslide and glacier dynamics at finer scale are required to conclude on the controlling factors of the landslide kinematics following the onset of glacier ice loss.

6. Conclusions

The analysis of a unique combination of time-series of ground elevation changes over 75 years, together with horizontal ground diplacement over 32 years, and a catalog of seismicity over 25 years, revealed the development of a very large slow-moving landslide on the flank of Tungnakvíslarjökull glacier, in relation with the glacier-retreat. Our results, in particular the analysis of the seismicity location, the compatibility of the waveforms and magnitudes with landslide processes, the clear time-relation between the seismic and landslide activity, clearly identify the landslide dynamics as the source of the shallow seismicity, and close a controversy of 15 years on its origin.

The time-series of ground displacement reveal a slow motion of the landslide since at least 1945, with a slight acceleration in the first years of the glacier-retreat. This acceleration is associated with a decrease of the rupture size along the fault, that we interpret as a progressive landslide mass segmentation. A transient acceleration phase occurred suddenly 6 years after the onset of the glacier retreat, and lasted 4 years. Our results clearly indicate that debuttressing of the slope due to glacier-retreat is the main cause of the landslide acceleration, associated with a decrease of the mechanical properties of the slope followed by a rapid time-response of the slope motion to this debuttressing. Despite the segmentation of the landslide mass that can favor groundwater infiltrations, our results preclude the groundwater as the final trigger of this transient motion. This questions the controlling factors of the glacier buttressing on the slope, in particular the viscosity of the ice at low strain-rates, or the glacier basal friction that can evolve interannually and seasonally. Further simultaneous measurements of landslide and glacier dynamics must be realized using local seismic networks and GNSS to better decipher these controlling factors.

Data Availability Statement

All satellite data used in this study are publicly accessible. The Landsat-7/8 images are available on the USGS Earthexplorer website (https://earthexplorer.usgs.gov/). The SPOT1 image is available on the catalog Regards (https://regards.cnes.fr/user/swh/modules/8). The ASTER images are available through NASA EarthData search (https://search.earthdata.nasa.gov/). The aerial photographs from 1945 to 1994 are openly available at www.lmi.is. The SIL catalog and climatological data are openly available at www.vedur.is. The softwares used to produce the DEMs and the time-series of horizontal displacement are available for download online. The mic-mac software is available at https://micmac.ensg.eu/index.php/Accueil. The cosi-corr module is available at www.tectonics.caltech.edu/slip_history/spot_coseis/download_software.html. The TIO module is available at https://sourcesup.renater.fr/www/tio/. The AMES stereo pipeline is available at https://ti.arc.nasa.gov/tech/asr/groups/intelligent-robotics/ngt/stereo/. The time-series of DEMs derived from ASTER, velocity maps, fitted dh/dt map of 2000–2020, fitted velocities of 1999–2019 and filtered seismic data from the SIL network are openly available in the Zenodo repository associated to this work (Lacroix et al., 2022): https://zenodo.org/record/6397629.

Acknowledgments
P. Lacroix deeply thank Mathieu Causse and François Renard for all the interesting discussions on the analysis of the seismic data set, and Andreas Kääb and François Renard for the invitation at the University of Oslo. We thank Bryndís Brandsdóttir for providing the seismic data used in this study. E. Berthier and P. Lacroix acknowledge the support from the French Space Agency (CNES) through the TOSCA, PNTS, SPOT World Heritage and ISIS programs.

References

Abercrombie, R. E. (2021). Resolution and uncertainties in estimates of earthquake stress drop and energy release. *Philosophical Transactions of the Royal Society A*, *379*(2196), 20200131. https://doi.org/10.1098/rsta.2020.0131

Abercrombie, R. E., Bannister, S., Ristau, J., & Doser, D. (2016). Variability of earthquake stress drop in a subduction setting, the Hikurangi margin, New Zealand. *Geophysical Journal International*, *208*(1), 306–320. https://doi.org/10.1093/gji/ggw393

Ágústsson, H., Hannesdóttir, H., Thorsteinsson, T., Pálsson, F., & Oddsson, B. (2013). Mass balance of Mýrdalsjökull ice cap accumulation area and comparison of observed winter balance with simulated precipitation. *Jökull Journal*, *63*, 91–104.

Aki, K. (1966). Generation and propagation of g waves from the Niigata earthquake of June 16, 1964: Part 2. Estimation of earthquake moment, released energy, and stress-strain drop from the g wave spectrum. *Bulletin of the Earthquake Research Institute, University of Tokyo*, *44*(1), 73–88.

Allmann, B. P., & Shearer, P. M. (2009). Global variations of stress drop for moderate to large earthquakes. *Journal of Geophysical Research*, *114*(B1). https://doi.org/10.1029/2008jb005821

Aðalgeirsdóttir, G., Magnússon, E., Pálsson, F., Thorsteinsson, T., Belart, J., Jóhannesson, T., et al. (2020). Glacier changes in Iceland from 1890 to 2019. *Frontiers of Earth Science*, *8*, 520. https://doi.org/10.3389/feart.2020.523646

Ballantyne, C. K., & Stone, J. O. (2004). The Beinn Alligin rock avalanche, NW Scotland: Cosmogenic 10be dating, interpretation and significance. *The Holocene*, *14*(3), 448–453. https://doi.org/10.1191/0959683604hl720rr

Belart, J., Magnússon, E., Berthier, E., Gunnlaugsson, Á., Pálsson, F., Adalgeirsdóttir, G., et al. (2020). Mass balance of 14 Icelandic glaciers, 1945–2017: Spatial variations and links with climate. *Frontiers of Earth Science*, *8*, 163. https://doi.org/10.3389/feart.2020.00163

Belart, J., Magnusson, E., Berthier, E., Pálsson, F., Adalgeirsdóttir, G., & Jóhannesson, T. (2019). The geodetic mass balance of Eyjafjallajökull ice cap for 1945–2014: Processing guidelines and relation to climate. *Journal of Glaciology*, *65*(251), 395–409. https://doi.org/10.1017/jog.2019.16

Ben-Yehoshua, D., Sæmundsson, Þ., Helgason, J. K., Belart, J. M., Sigurðsson, J. V., & Erlingsson, S. (2022). Paraglacial exposure and collapse of glacial sediment: The 2013 landslide onto Svínafellsjökull, Southeast Iceland. *Earth Surface Processes and Landforms*. https://doi.org/10.1002/esp.5398

Berthier, E., Arnaud, Y., Kumar, R., Ahmad, S., Wagnon, P., & Chevallier, P. (2007). Remote sensing estimates of glacier mass balances in the Himachal Pradesh (Western Himalaya, India). *Remote Sensing of Environment*, *108*(3), 327–338. https://doi.org/10.1016/j.rse.2006.11.017

Björnsson, H., Pálsson, F., & Guðmundsson, M. T. (2000). Surface and bedrock topography of the Mýrdalsjökull ice cap. *Jökull Journal*, *49*, 29–46.

Bontemps, N., Lacroix, P., & Doin, M.-P. (2018). Inversion of deformation fields time-series from optical images, and application to the long term kinematics of slow-moving landslides in Peru. *Remote Sensing of Environment*, *210*, 144–158. https://doi.org/10.1016/j.rse.2018.02.023

Bontemps, N., Lacroix, P., Larose, E., Jara, J., & Taipe, E. (2020). Rain and small earthquakes maintain a slow-moving landslide in a persistent critical state. *Nature Communications*, *11*(1), 1–10. https://doi.org/10.1038/s41467-020-14445-3

Brun, F., Berthier, E., Wagnon, P., Kääb, A., & Treichler, D. (2017). A spatially resolved estimate of high mountain Asia glacier mass balances from 2000 to 2016. *Nature Geoscience*, *10*(9), 668–673. https://doi.org/10.1038/ngeo2999

Chiarle, M., Geertsema, M., Mortara, G., & Clague, J. J. (2021). Relations between climate change and mass movement: Perspectives from the Canadian Cordillera and the European Alps. *Global and Planetary Change*, *202*, 103499. https://doi.org/10.1016/j.gloplacha.2021.103499

Clarke, G. K. (2005). Subglacial processes. *Annual Review of Earth and Planetary Sciences*, *33*(1), 247–276. https://doi.org/10.1146/annurev.earth.33.092203.122621

Cook, K. L., Andermann, C., Gimbert, F., Adhikari, B. R., & Hovius, N. (2018). Glacial lake outburst floods as drivers of fluvial erosion in the Himalaya. *Science*, *362*(6410), 53–57. https://doi.org/10.1126/science.aat4981

Cook, K. L., Rekapalli, R., Dietze, M., Pilz, M., Cesca, S., Rao, N. P., et al. (2021). Detection and potential early warning of catastrophic flow events with regional seismic networks. *Science*, *374*(6563), 87–92. https://doi.org/10.1126/science.abj1227

Cruden, D., & Hu, X. (1993). Exhaustion and steady state models for predicting landslide hazards in the Canadian Rocky Mountains. *Geomorphology*, *8*(4), 279–285. https://doi.org/10.1016/0169-555X(93)90024-V

Dai, C., Higman, B., Lynett, P. J., Jacquemart, M., Howat, I. M., Liljedahl, A. K., et al. (2020). Detection and assessment of a large and potentially tsunamigenic periglacial landslide in Barry arm, Alaska. *Geophysical Research Letters*, *47*(22), e2020GL089800. https://doi.org/10.1029/2020gl089800

Dehecq, A., Gourmelen, N., Gardner, A. S., Brun, F., Goldberg, D., Nienow, P. W., et al. (2019). Twenty-first century glacier slowdown driven by mass loss in high mountain Asia. *Nature Geoscience*, *12*(1), 22–27. https://doi.org/10.1038/s41561-018-0271-9

Deparis, J., Jongmans, D., Cotton, F., Baillet, L., Thouvenot, F., & Hantz, D. (2008). Analysis of rock-fall and rock-fall avalanche seismograms in the French Alps. *Bulletin of the Seismological Society of America*, *98*(4), 1781–1796. https://doi.org/10.1785/0120070082

Evans, S. G., & Clague, J. J. (1994). Recent climatic change and catastrophic geomorphic processes in mountain environments. In *Geomorphology and natural hazards* (pp. 107–128). Elsevier.

Gardelle, J., Berthier, E., Arnaud, Y., & Kääb, A. (2013). Region-wide glacier mass balances over the Pamir-Karakoram-Himalaya during 1999–2011. *The Cryosphere*, *7*(4), 1263–1286. https://doi.org/10.5194/tc-7-1263-2013

Girod, L., Nuth, C., Kääb, A., McNabb, R., & Galland, O. (2017). MMASTER: Improved ASTER DEMS for elevation change monitoring. *Remote Sensing*, *9*(7), 704. https://doi.org/10.3390/rs9070704

Glueer, F., Loew, S., Manconi, A., & Aaron, J. (2019). From toppling to sliding: Progressive evolution of the Moosfluh Landslide, Switzerland. *Journal of Geophysical Research: Earth Surface*, *124*(12), 2899–2919. https://doi.org/10.1029/2019jf005019

Grämiger, L. M., Moore, J. R., Gischig, V. S., Ivy-Ochs, S., & Loew, S. (2017). Beyond debuttressing: Mechanics of paraglacial rock slope damage during repeat glacial cycles. *Journal of Geophysical Research: Earth Surface*, *122*(4), 1004–1036. https://doi.org/10.1002/2016jf003967

Hannesdóttir, H., Sigurðsson, O., Þrastarson, R. H., Guðmundsson, S., Belart, J. M., Pálsson, F., et al. (2020). A national glacier inventory and variations in glacier extent in Iceland from the Little Ice Age maximum to 2019. *Jökull Journal*, *70*, 1–34. https://doi.org/10.33799/jokull.70.001

Heid, T., & Kääb, A. (2012). Repeat optical satellite images reveal widespread and long term decrease in land-terminating glacier speeds. *The Cryosphere*, *6*(2), 467–478. https://doi.org/10.5194/tc-6-467-2012

Helmstetter, A., & Garambois, S. (2010). Seismic monitoring of Sechilienne rockslide (French Alps): Analysis of seismic signals and their correlation with rainfalls. *Journal of Geophysical Research*, *115*(F3), 15. https://doi.org/10.1029/2009JF001532

Hilger, P., Hermanns, R. L., Czekirda, J., Myhra, K. S., Gosse, J. C., & Etzelmüller, B. (2021). Permafrost as a first order control on long-term rock-slope deformation in (sub-) Arctic Norway. *Quaternary Science Reviews*, *251*, 106718. https://doi.org/10.1016/j.quascirev.2020.106718

Huggel, C., Clague, J. J., & Korup, O. (2012). Is climate change responsible for changing landslide activity in high mountains? *Earth Surface Processes and Landforms*, *37*(1), 77–91. https://doi.org/10.1002/esp.2223

Hugonnet, R., McNabb, R., Berthier, E., Menounos, B., Nuth, C., Girod, L., et al. (2021). Accelerated global glacier mass loss in the early twenty-first century. *Nature*, *592*(7856), 726–731. https://doi.org/10.1038/s41586-021-03436-z

Johannesson, T., Björnsson, H., Magnusson, E., Gudmundsson, S., Palsson, F., Sigurdsson, O., et al. (2013). Ice-volume changes, bias estimation of mass-balance measurements and changes in subglacial lakes derived by Lidar mapping of the surface of Icelandic glaciers. *Annals of Glaciology*, *54*(63), 63–74. https://doi.org/10.3189/2013aog63a422

Jónsdóttir, K., Roberts, R., Pohjola, V., Lund, B., Shomali, Z. H., Tryggvason, A., & Bövarsson, R. (2009). Glacial long period seismic events at Katla volcano, Iceland. *Geophysical Research Letters*, *36*(11), L11402. https://doi.org/10.1029/2009gl038234

Jónsdóttir, K., Tryggvason, A., Roberts, R., Lund, B., Soosalu, H., & Bövarsson, R. (2007). Habits of a glacier-covered volcano: Seismicity patterns and velocity structure of Katla volcano, Iceland. *Annals of Glaciology*, *45*, 169–177. https://doi.org/10.3189/172756407782282499

Kos, A., Amann, F., Strozzi, T., Delaloye, R., von Ruette, J., & Springman, S. (2016). Contemporary glacier retreat triggers a rapid landslide response, Great Aletsch Glacier, Switzerland. *Geophysical Research Letters*, *43*(24), 12–466. https://doi.org/10.1002/2016gl071708

Lacasse, C., & Garbe-Schönberg, C.-D. (2001). Explosive silicic volcanism in Iceland and the Jan Mayen area during the last 6 Ma: Sources and timing of major eruptions. *Journal of Volcanology and Geothermal Research*, *107*(1–3), 113–147. https://doi.org/10.1016/s0377-0273(00)00299-7

Lacroix, P., & Amitrano, D. (2013). Long-term dynamics of rockslides and damage propagation inferred from mechanical modeling. *Journal of Geophysical Research: Earth Surface*, *118*(4), 2292–2307. https://doi.org/10.1002/2013JF002766

Lacroix, P., Araujo, G., Hollingsworth, J., & Taipe, E. (2019). Self-entrainment motion of a slow-moving landslide inferred from Landsat-8 time series. *Journal of Geophysical Research: Earth Surface*, *124*(5), 1201–1216. https://doi.org/10.1029/2018jf004920

Lacroix, P., Belart, J. M., Berthier, E., Sæmundsson, Þ., & Jónsdóttir, K. (2022). Mechanism of landslide induced by glacier-retreat on the Tungnakvíslarjökull area. *Zenodo*. https://doi.org/10.5281/zenodo.6397629

Lacroix, P., Dehecq, A., & Taipe, E. (2020). Irrigation-triggered landslides in a Peruvian desert caused by modern intensive farming. *Nature Geoscience*, *13*(1), 56–60. https://doi.org/10.1038/s41561-019-0500-x

Lacroix, P., Handwerger, A. L., & Bièvre, G. (2020). Life and death of slow-moving landslides. *Nature Reviews Earth & Environment*, *1*(8), 1–16. https://doi.org/10.1038/s43017-020-0072-8

Le Breton, M., Bontemps, N., Guillemot, A., Baillet, L., & Larose, É. (2021). Landslide monitoring using seismic ambient noise correlation: Challenges and applications. *Earth-Science Reviews*, *216*, 103518. https://doi.org/10.1016/j.earscirev.2021.103518

Leprince, S., Barbot, S., Ayoub, F., & Avouac, J.-P. (2007). Automatic and precise orthorectification, coregistration, and Subpixel correlation of satellite images, application to ground deformation measurements. *IEEE Transactions on Geoscience and Remote Sensing*, *45*(6), 1529–1558. https://doi.org/10.1109/TGRS.2006.888937

Li, S., Li, C., Yao, D., & Liu, C. (2020). Interdisciplinary asperity theory to analyze nonlinear motion of loess landslides with weak sliding interface. *Landslides*, *17*(12), 2957–2965. https://doi.org/10.1007/s10346-020-01479-3

Manighetti, I., Campillo, M., Bouley, S., & Cotton, F. (2007). Earthquake scaling, fault segmentation, and structural maturity. *Earth and Planetary Science Letters*, *253*(3–4), 429–438. https://doi.org/10.1016/j.epsl.2006.11.004

McColl, S. T. (2012). Paraglacial rock-slope stability. *Geomorphology*, *153*, 1–16. https://doi.org/10.1016/j.geomorph.2012.02.015

McColl, S. T., & Davies, T. R. (2013). Large ice-contact slope movements: Glacial buttressing, deformation and erosion. *Earth Surface Processes and Landforms*, *38*(10), 1102–1115. https://doi.org/10.1002/esp.3346

Poli, P. (2017). Creep and slip: Seismic precursors to the Nuugaatsiaq landslide (Greenland). *Geophysical Research Letters*, *44*(17), 8832–8836. https://doi.org/10.1002/2017gl075039

Provost, F., Malet, J.-P., Hibert, C., Helmstetter, A., Radiguet, M., Amitrano, D., et al. (2018). Towards a standard typology of endogenous landslide seismic sources. *Earth Surface Dynamics*, *6*(4), 1059–1088. https://doi.org/10.5194/esurf-6-1059-2018

Rosenau, R., Scheinert, M., & Dietrich, R. (2015). A processing system to monitor Greenland outlet glacier velocity variations at decadal and seasonal time scales utilizing the Landsat imagery. *Remote Sensing of Environment*, *169*, 1–19. https://doi.org/10.1016/j.rse.2015.07.012

Rupnik, E., Daakir, M., & Deseilligny, M. P. (2017). MicMac–a free, open-source solution for photogrammetry. *Open Geospatial Data, Software and Standards*, *2*(1), 1–9. https://doi.org/10.1186/s40965-017-0027-2

Shean, D. E., Alexandrov, O., Moratto, Z. M., Smith, B. E., Joughin, I. R., Porter, C., & Morin, P. (2016). An automated, open-source pipeline for mass production of digital elevation models (DEMs) from very-high-resolution commercial stereo satellite imagery. *ISPRS Journal of Photogrammetry and Remote Sensing*, *116*, 101–117. https://doi.org/10.1016/j.isprsjprs.2016.03.012

Soldati, M., Corsini, A., & Pasuto, A. (2004). Landslides and climate change in the Italian Dolomites since the Late glacial. *CATENA*, *55*(2), 141–161. https://doi.org/10.1016/S0341-8162(03)00113-9

Soosalu, H., Jónsdóttir, K., & Einarsson, P. (2006). Seismicity crisis at the Katla volcano, Iceland—Signs of a cryptodome? *Journal of Volcanology and Geothermal Research*, *153*(3–4), 177–186. https://doi.org/10.1016/j.jvolgeores.2005.10.013

Spaans, K., Hreinsdóttir, S., Hooper, A., & Ófeigsson, B. G. (2015). Crustal movements due to Iceland's shrinking ice caps mimic magma inflow signal at Katla volcano. *Scientific Reports*, *5*(1), 1–8. https://doi.org/10.1038/srep10285

Spreafico, M. C., Sternai, P., & Agliardi, F. (2021). Paraglacial rock-slope deformations: Sudden or delayed response? Insights from an integrated numerical modelling approach. *Landslides*, *18*(4), 1311–1326. https://doi.org/10.1007/s10346-020-01560-x

Storni, E., Hugentobler, M., Manconi, A., & Loew, S. (2020). Monitoring and analysis of active rockslide-glacier interactions (Moosfluh, Switzerland). *Geomorphology*, *371*, 107414. https://doi.org/10.1016/j.geomorph.2020.107414

Torfason, H., & Jónsson, H. (2005). Jarðfræði við norðvestaverðan Mýrdalsjökul (geology of the area to the northwest of Mýrdalsjökull). *Hættumat vegna eldgosa og hlaupa frá Vestanverðum Mýrdalsjökli og Eyjafjallajökli (Assessment of Risk Due to Volcanic Eruptions and Jökulhlaups from Western Mýrdalsjökull and Eyjafjallajökull)*, 45–73.

Yamada, M., Mori, J., & Matsushi, Y. (2016). Possible stick-slip behavior before the Rausu landslide inferred from repeating seismic events. *Geophysical Research Letters*, *43*(17), 9038–9044. https://doi.org/10.1002/2016gl069288

Zemp, M., Huss, M., Thibert, E., Eckert, N., McNabb, R., Huber, J., et al. (2019). Global glacier mass changes and their contributions to sea-level rise from 1961 to 2016. *Nature*, *568*(7752), 382–386. https://doi.org/10.1038/s41586-019-1071-0

Zerathe, S., Lebourg, T., Braucher, R., & Bourlès, D. (2014). Mid-Holocene cluster of large-scale landslides revealed in the Southwestern Alps by 36CL dating. Insight on an Alpine-scale landslide activity. *Quaternary Science Reviews*, *90*, 106–127. https://doi.org/10.1016/j.quascirev.2014.02.015